The Onset of Calcium Carbonate Nucleation: A Density Functional Theory Molecular Dynamics and Hybrid Microsolvation/Continuum Study

ARTICLE *in* THE JOURNAL OF PHYSICAL CHEMISTRY B · JULY 2008

Impact Factor: 3.3 · DOI: 10.1021/jp801070b · Source: PubMed

2 AUTHORS:

Di Tommaso Devis
Queen Mary, University of London
34 PUBLICATIONS **555** CITATIONS
SEE PROFILE

Nora H. de Leeuw
Cardiff University
240 PUBLICATIONS **4,431** CITATIONS
SEE PROFILE

The Onset of Calcium Carbonate Nucleation: A Density Functional Theory Molecular Dynamics and Hybrid Microsolvation/Continuum Study

Devis Di Tommaso* and Nora H. de Leeuw

Department of Chemistry, Christopher Ingold Laboratories, University College London, 20 Gordon Street, London WC1H OAJ, United Kingdom

Received: February 5, 2008; Revised Manuscript Received: March 10, 2008

Density functional theory (Perdew−Burke−Ernzerhof) based methods have been used to study the structure and hydration environment of the building blocks of $CaCO_3$ in aqueous solutions of calcium bicarbonate and calcium carbonate. Car−Parrinello molecular dynamics simulations of Ca^{2+}/CO_3^{2-} and Ca^{2+}/HCO_3^- in explicit water were performed to investigate the formation of $CaCO_3$ and the hydration shell of the solvated hetero-ion pair. Our simulations show that the formation of the monomer of $CaCO_3$ occurs with an associative mechanism and that the dominant building block of calcium (bi)carbonate in aqueous solution is $Ca[\eta^1\text{-}(H)CO_3](H_2O)_5$, i.e., the preferred hydration number is five, while the (bi)carbonate is coordinated to the calcium in a monodentate mode. This result agrees with static calculations, where a hybrid approach using a combination of explicit solvent molecules and a polarizable continuum model has been applied to compute the solvation free energies of calcium bicarbonate species. Furthermore, the discrete-continuum calculations predict that the $Ca(HCO_3)_2$ and $Ca(HCO_3)_3^-$ species are stable in an aqueous environment preferentially as $Ca(HCO_3)_2(H_2O)_4$ and $Ca(HCO_3)_3(H_2O)_2^-$, respectively.

I. Introduction

The formation of calcium carbonate ($CaCO_3$) from supersaturated solutions has been studied for more than a century as it represents a process of considerable geochemical, biological, and industrial importance. Moreover, the precipitation of calcium carbonate minerals from the reaction of Ca-silicate mineral oxides like wollastonite ($CaSiO_3$) or anorthite ($CaAl_2Si_2O_8$) with CO_2 represents a potential route to the capture and sequestration of CO_2 and the mitigation of carbon dioxide-caused climate change (e.g., $CaSiO_3 + CO_2 + 2H_2O \rightarrow CaCO_3 + H_4SiO_4$).[1] The carbonation process includes two distinct reactions: silicate mineral dissolution followed by carbonate precipitation. A considerable number of publications have been concerned with the nucleation of calcium carbonate minerals and it is now understood that the first step in the mineralization of $CaCO_3$ is the homogeneous nucleation of amorphous particles, which represent a transient precursor phase in the formation of more stable crystalline polymorphs of $CaCO_3$ (calcite, vaterite, or aragonite).[2] Computational modeling at the atomistic level has been extensively used to study the growth of calcium carbonate in a wide variety of situations, which include the use of organic templates to control the growth and morphology of calcium carbonate,[3] the effect of phosphates and phosphonates on calcite nucleation and growth,[4] and calcite crystal growth inhibition by organic acids and aldehydes,[5] to give only a few examples. Surprisingly, a theoretical study on the process of calcium carbonate nucleation from homogeneous aqueous solution is still missing. The understanding of the early stages of this phenomenon would shed light on a process that is of fundamental interest as much to the geological and life sciences as it is to technology.

Although much attention has been devoted to a theoretical analysis of Ca^{2+} in water,[6] only recently has the first force field classical molecular dynamics (MD) study been conducted on calcium carbonate in water,[7] where the authors considered the hydration properties of Ca^{2+}, CO_3^{2-}, and a single unit of $CaCO_3$. However, in more common situations like natural waters and in solutions below pH 10.3 the bicarbonate HCO_3^- anions are predominant.[8]

The purpose of the present paper is to draw a clear picture of the structure and hydration environment of the building blocks (monomers) of $CaCO_3$ in calcium bicarbonate and calcium carbonate aqueous solutions. The definition of the most stable monomer of calcium carbonate is essential for the modeling of the nucleation process of $CaCO_3$ using first principle methods.[9,10]

Because in aqueous solution calcium carbonate species are likely to participate in reactions involving the exchange of protons with its protonated species (e.g., $CaHCO_3^+ + H_2O \leftrightarrow CaCO_3 + H_3O^+$), quantum mechanical techniques are the preferred methods to investigate these processes. Therefore, we decided to undertake an extensive investigation of the structure and energetic properties of calcium (bi)carbonates in water using density functional theory (DFT) based approaches. We have conducted Car−Parrinello (CP)[11] molecular dynamics simulations of Ca^{2+} and HCO_3^- in water to investigate the formation of $CaCO_3$ and the hydration shell of the solvated hetero-ion pair. In the CP-DFT method the electronic structure is explicitly taken into account, which enables the accurate modeling of many-body and polarization effects, but at the expense of much larger computational requirements compared to classical MD simulations. For this reason it is difficult to perform simulations large enough to yield thermodynamic averages. Therefore, we have decided to complement the CPMD simulations with static DFT calculations using a hybrid microsolvation/continuum approach[12] to study the structure and stability of calcium bicarbonate $[Ca(HCO_3)_m(H_2O)_n]^{2-m}$ species in aqueous solution. In this hybrid method the water molecules in the first solvation shell of calcium have been explicitly considered while the remainder of the bulk solvent is treated as a dielectric continuum.

* Author to whom correspondence should be adressed. E-mail: uccaddi@ucl.ac.uk.

10.1021/jp801070b CCC: $40.75

Published on Web 05/14/2008

Within this framework, the solvation free energies of calcium bicarbonates in water have been computed to identify the species present in solution and to assess their stability.

In this paper, having described the computational details of the CPMD and static ab initio calculations in the Methods section, we first consider an assessment of the DFT level used in the present study, before discussing the CPMD simulations on the $Ca^{2+}-(H)CO_3^-$−water system. Finally, we present the structures and stabilities of $[Ca(HCO_3)_m(H_2O)_n]^{2-m}$ clusters immersed in a dielectric continuum solvation field.

II. Methods

A. Car−Parrinello Molecular Dynamics Simulations. Car−Parrinello (CP) molecular dynamics calculations were carried out using the CP code included in the Quantum-ESPRESSO package, version 3.2,[13] which implements density functional theory (DFT) using a plane-wave (PW) basis set and pseudopotentials approach. We used the Perdew−Burke−Ernzerhof (PBE)[14] generalized gradient approximation (GGA) for the exchange and correlation terms. Vanderbilt ultrasoft pseudopotentials (US)[15] represented core−valence interactions for all atomic species; semicore shells were explicitly included for Ca. The accuracy and transferability of the pseudopotentials were previously tested by comparing the optimized structure of several molecules and crystals containing Ca and O atoms with the corresponding experimental values, as well as with the corresponding theoretical values calculated with similar approximations.[16] Plane-wave basis set cutoffs for the smooth part of the wave functions and the augmented density were set to 30 and 200 Ry, respectively, which ensured convergence in the above test calculations. *k*-sampling was restricted to the Γ point of the Brillouin zone. To further validate our US-PW approach we used the PWSCF code, which is also part of the Quantum-ESPRESSO package,[13] to calculate the structure and the hydration energies of $Ca(OH)_2(H_2O)_n$, $Ca(H_2O)_n^{2+}$ and $Ca(HCO_3)(H_2O)_n^+$ gas-phase complexes. For these calculations we used a cubic supercell with 15 Å sides. In the CPMD simulations, the hydrogen nuclei were treated as classical particles with the mass of the deuterium isotope, and the fictitious electron mass μ was set equal to 600 au. The choice of these parameters is consistent with the ratio $\mu/M \leq 1/3$ suggested by Grossman when investigating the structural properties of aqueous solution.[17] The time step was set equal to 0.14 fs, and all simulations were carried out in the NVT ensemble, using a single Nose-Hoover thermostat with an estimated time constant of 21.5 fs to maintain the average temperature at $T = 400$ K. Previous CPMD simulations have shown that the underlying PBE functional yields overstructured water compared to experiment and slow dynamics at $T = 300$ K, suggesting that the freezing point of water is around 400 K.[18,19] A higher temperature is therefore necessary to obtain a reasonable liquid-like water structure and diffusion time scales in CP and Born−Oppenheimer molecular dynamic simulations employing the PBE functional.[20] Hence our choice of $T = 400$ K for the simulations (see also discussion in Section IIIB). To create the initial configuration of the $Ca^{2+}-HCO_3^-$−water system we started from a CP simulation on 54 water molecules in a cubic supercell with a side length of 11.53 Å. Starting from the last configuration, one water was replaced with Ca^{2+} and the simulation was run for 5 ps to create the first and second coordination spheres around the cation. At this point, a bicarbonate ion was placed in the second coordination sphere of Ca^{2+}, i.e., $r(Ca-O_c) \approx 4.8$ Å. The initial geometry of HCO_3^- was obtained from a gas-phase optimization at the DFT-PBE level of theory. We considered two different ways to compensate for the excess of positive charge: (i) one water molecule was replaced with OH^-, and the simulation cell consisted of 51 water molecules and 1 OH^-, 1 HCO_3^-, and 1 Ca^{2+} ions (simulation A) and (ii) a jellium background was inserted to remove divergences, due to the cell being charged, and the simulation cell consisted of 52 water molecules plus 1 HCO_3^- and 1 Ca^{2+} ions (simulation B). To determine if the simulation conditions may have biased the results, two other simulation cells were considered, which consisted of 50 water molecules plus 1 OH^-, 1 HCO_3^-, and 1 Ca^{2+} ions in a cubic box with a side length of 11.74 Å. In these simulations the cation−anion pair was already formed (simulations C and D). Equilibration and production times relative to each simulation cell are specified in the Results and Discussion section. The radial distribution functions were collected with a bin size of 0.03.

B. Static Density Functional Theory Calculations. Static calculations on $[Ca(HCO_3)_m(H_2O)_n]^{2-m}$ gas-phase clusters, where $m = 1-3$ and $n = 0-6$, were performed with DMol^3, version 4.0, code[21,22] to optimize gas-phase geometries and compute frequencies. The electronic structure was described within the DFT-PBE approximation.[14] This enables direct comparison with the MD simulations. In DMol^3 the electronic wave function is expanded in a localized atom-centered basis set with each basis function defined numerically on a dense radial grid. We used all-electron double-numeric-polarized (DNP) basis sets on all atoms. This basis set is variationally comparable to the 6-31G(d,p) basis set. However, the numerical functions are far more complete than the traditional Gaussian functions. Because of the quality of these orbitals, basis set superposition effects (BSSE) are minimized[21] and it is possible to obtain an excellent description, even of weak bonds. Indeed, the numerical basis set is more spatially extended than the 6-31G(d,p) basis sets and is therefore able to describe the tail of the wave function due to the long-range interaction. Each basis function was restricted to a cutoff radius of $R_{cut} = 5.5$ Å. The electron density was approximated by using a multipolar expansion up to octupole. Frequency calculations were performed on the gas-phase $[Ca(HCO_3)_m(H_2O)_n]^{2-m}$ geometries to verify that no imaginary frequencies were present. Enthalpy and Gibbs free energy corrections were obtained with these frequency calculations.

The effect of the bulk water was estimated by using the conductor-like screening model (COSMO) variation of the self-consistent reaction field model[23] as implemented in DMol^3 (see ref 24) and the calculations have been performed on the gas-phase optimized geometries. To compute the hydration energy of the $[Ca(HCO_3)_m(H_2O)_n]^{2-m}$ species at ambient conditions we used a dielectric constant $\epsilon = 78.4$, which corresponds to water at 300 K. Note that this temperature differs from the average temperature maintained during the CPMD simulations, where the emphasis of the investigation was on the structure of the calcium (bi)carbonate in water and a higher temperature of 400 K was necessary to obtain a liquid-like behavior for the calcium (bicarbonate) solutions. To build the molecular shape cavity in the COSMO calculations we used the optimized Klamt atomic radii of 1.72 Å for oxygen, 1.30 Å for hydrogen, 2.00 Å for carbon,[25] and an atomic radius of 1.95 Å for the calcium atom.

The solvation free energies of $Ca(HCO_3)_m$ species within the discrete-continuum model have been computed from the thermodynamic cycle presented in Scheme 1, using the following expression[12] (S denotes the solute):

SCHEME 1

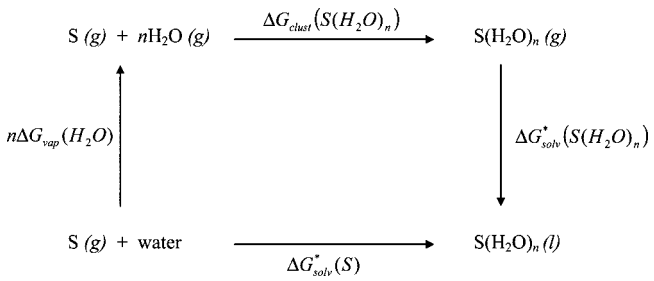

$$\Delta G^*_{\mathrm{solv}}(S) = \Delta G_{\mathrm{clust}}(S(\mathrm{H_2O})_n) + \Delta G^*_{\mathrm{solv}}(S(\mathrm{H_2O})_n) + n\Delta G_{\mathrm{vap}}(\mathrm{H_2O}) \quad (1)$$

In (eq 1) $\Delta G_{\mathrm{clust}}(S(\mathrm{H_2O})_n)$ is the gas-phase free energy of cluster formation at 1 atm, $\Delta G^*_{\mathrm{solv}}(\mathrm{S(H_2O)}_n)$ is the solvation free energy of the hydrated cluster corresponding to the 1 mol L^{-1} (gas) → 1 mol L^{-1} (sol) process, and $\Delta G_{\mathrm{vap}}(\mathrm{H_2O})$ is the vaporization free energy of a single water molecule, which is calculated as[12]

$$\Delta G_{\mathrm{vap}}(\mathrm{H_2O}) = -\Delta G^*_{\mathrm{solv}}(\mathrm{H_2O}) - RT\ln[\tilde{R}T] - RT\ln[\mathrm{H_2O}] \quad (2)$$

where $\tilde{R} = 0.082053\ \mathrm{K^{-1}}$. The solvation free energy of the water molecule, $\Delta G_{\mathrm{solv}}(\mathrm{H_2O})$, determined by the COSMO model is 5.2 kcal $\mathrm{mol^{-1}}$ and taking $[\mathrm{H_2O}] = 55.5$ mol L^{-1}, eq 2 gives a vaporization energy, $\Delta G_{\mathrm{vap}}(\mathrm{H_2O})$, of 1.0 kcal $\mathrm{mol^{-1}}$.

To assess the quality of the DMol^3-PBE method we have also performed a complementary study on the structure and binding energy of the $[\mathrm{Ca(H_2O)_6}]^{2+}$ complex. In these calculations, the VWN[26] and BLYP[27] functionals were also tested and the results were compared with Gaussian 03 calculations,[28] where we considered a certain hierarchy for the Gaussian basis set [6-31G(d,p), 6-31++G(d,p), 6-311G(2d,2p), 6-311++G-(2d,2p), aug-cc-pVTZ for H, O and cc-pVTZ for Ca][29] along with the PBE method and two hybrid-meta-DFT (HMDFT) functionals, mPW1B95 and mPWB1K.[30] We have in particular chosen mPW1B95 because this density functional has been specifically developed for thermochemistry calculation and its assessment against a representative database of molecular properties showed that this method is one of the best tested density functionals for the accurate calculation of thermochemical properties.[31] Calculations have also been performed at the ab initio HF and MP2 levels of theory. In the HF geometry optimization we used the 86-511d3G basis set for calcium,[32] while oxygen and hydrogen have been represented by a 6-31G(d,p) basis set with the outer shell exponents $\alpha_{sp} = 0.2742$ and 1.0 $\mathrm{bohr^{-2}}$, $\alpha_{sp} = 0.538$ $\mathrm{bohr^{-2}}$ for O, and $\alpha_{sp} = 0.1613$ $\mathrm{bohr^{-2}}$, $\alpha_p = 1.1$ $\mathrm{bohr^{-2}}$ for H.[33] This basis set will be referred to as BS-HF.

III. Results and Discussion

A. Assessment of the Method. The aim of this section is to assess the DFT-PBE methods used in the present study by considering the effect of the exchange-correlation and of the basis set on the geometry and energetics of the class of compounds under investigation.

We start by comparing in Table 1 the structure and the hydration energy of the first solvation shell, $\Delta E = E[\mathrm{S(H_2O)}_n] - \mathrm{E[S]} - n\mathrm{E[H_2O]}$, of the $\mathrm{Ca(OH)_2(H_2O)}_n$, $\mathrm{Ca(H_2O)}_n{}^{2+}$, and $[\mathrm{Ca(HCO_3)(H_2O)}_n]^+$ clusters optimized by using the pseudopotential PWSCF-PBE/US-PW and the all-electron DMol^3-PBE/DNP methods. The calculated gas-phase geometries show good

TABLE 1: Optimized Structure (distances in Å and angles in deg), Hydration Energy of the First Solvation Shell, ΔE, and Successive Water Binding Energy, ΔE_{inc} (in kcal $\mathrm{mol^{-1}}$), of the $\mathrm{Ca(OH)_2(H_2O)}_n$, $\mathrm{Ca(H_2O)}_n{}^{2+}$, and $\mathrm{Ca(HCO_3)(H_2O)}_n{}^+$ Clusters Computed with Use of the PBE/US-PW and PBE/DNP Methods[a]

	r(Ca−OH)		r(Ca−O$_w$)		r(Ca−O$_c$)		r(O−H)		θ(H−O−H)		r(C−O)		θ (O−C−O)		ΔE		ΔE$_{inc}$	
	DNP	PW	DNP	PW	DNP	PW	DNP	PW	DNP	PW	DNP	PW	DNP	PW	DNP	PW	DNP	PW
H_2O							0.97	0.99	104.0	104.5								
$Ca(OH)_2$	2.03	2.03													−24.1	−22.6		
$Ca(OH)_2(H_2O)$	2.02	2.02	2.34	2.33			1.01	1.03	112.3	111.3					−45.0	−42.0	−20.9	−19.4
$Ca(OH)_2(H_2O)_2$	2.02	2.01	2.40	2.39			1.00	1.02	108.2	109.4								
$Ca(H_2O)^{2+}$			2.23	2.19			0.99	1.00	103.5	104.8					−56.6	−61.6		
$Ca(H_2O)_2{}^{2+}$			2.28	2.26			0.98	1.00	103.6	104.6					−105.6	−111.1	−49.0	−49.5
$Ca(H_2O)_3{}^{2+}$			2.31	2.28			0.98	0.99	103.6	104.7					−149.0	−157.0	−43.4	−45.8
$Ca(H_2O)_4{}^{2+}$			2.34	2.31			0.98	0.99	103.9	104.8					−187.1	−195.0	−38.0	−39.0
$Ca(H_2O)_5{}^{2+}$			2.38	2.35			0.98	0.99	104.4	105.2					−217.6	−224.2	−30.5	−29.2
$Ca(H_2O)_6{}^{2+}$			2.41	2.38			0.98	0.99	104.7	105.5					−245.3	−250.7	−27.7	−26.5
$CaHCO_3{}^+$					2.15	2.14					1.28	1.29	119.9	120.0				
$Ca(HCO_3)(H_2O)^+$			2.35	2.33	2.19	2.18	0.98	0.99	105.	105.8	1.29	1.29	120.7	120.9	−31.0	−30.6		
$Ca(HCO_3)(H_2O)_2{}^+$			2.37	2.36	2.22	2.22	0.98	0.99	105.3	106.3	1.29	1.29	121.5	121.7	−59.9	−58.2	−28.8	−27.6
$Ca(HCO_3)(H_2O)_3{}^+$			2.37	2.36	2.28	2.27	0.98	0.99	106.3	107.2	1.28	1.28	121.9	122.2	−85.2	−82.9	−25.3	−24.7

[a] The oxygen from water molecules is labeled O_w, the oxygen from bicarbonate is labeled O_c. $\Delta E = E[\mathrm{S(H_2O)}_n] - E[\mathrm{S}] - nE[\mathrm{H_2O}]$; $\Delta E_{\mathrm{inc}} = E[\mathrm{S(H_2O)}_{n+1}] - E[\mathrm{S(H_2O)}_n] - E[\mathrm{H_2O}]$.

TABLE 2: Optimized $r(Ca^{2+}-O)$ Internuclear Distance (in Å) and Hydration Energy of the First Solvation Shell, ΔE (in kcal mol^{-1}), of the Hexahydrated $Ca(H_2O)_6^{2+}$ Complex As Computed at the Various Levels of DFT and with the Different Basis Sets[a]

method	$r(Ca^{2+}-O)$	ΔE
VWN/DN	2.37	−303.7
VWN/DNP	2.33	−277.9
BLYP/DNP	2.43	−238.7
PBE/DN	2.45	−273.1
PBE/DND	2.48	−232.7
PBE/DNP	2.41	−245.3
PBE/6-31G(d,p)	2.43	−277.6
PBE/6-31++G(d,p)	2.45	−241.9
PBE/6-311G(2d,2p)//6-31++G(d,p)		−274.9
PBE/6-311++G(2d,2p)//6-31++G(d,p)		−243.5
PBE/cc-pVTZ//6-31++G(d,p)		−266.1
PBE/(aug-)cc-pVTZ[b]//6−31G(d,p)		−244.5
PBE/(aug-)cc-pVTZ[b]//6−31++G(d,p)		−243.8
PBE/(aug-)cc-pVTZ[b]//DNP		−244.6
PBE/(aug-)cc-pVTZ[b]	2.40	−244.6
mPWB1K/6-311++G(2d,2p)//6−31++G(d,p)	2.42	−244.9
mPW1B95/6-311++G(2d,2p)//6−31++G(d,p)	2.43	−243.5
mPW1B95/6-311++G(2d,2p)//PBE/DNP		−243.4
HF//(aug-)cc-pVTZ//BS-HF	2.40	−235.2
MP2/6-311++G(2d,2p)//PBE/DNP		−243.0

[a] $\Delta E = E[Ca(H_2O)_6^{2+}] - E[Ca^{2+}] - 6E[H_2O]$. [b] aug-cc-pVTZ for H, O and cc-pVTZ for Ca.

agreement: for the complexes $Ca(OH)_2(H_2O)_n$ and $Ca(HCO_3)(H_2O)_n^+$ the bond distances and bond angles differ by only 0.01 Å and 1°, respectively, while in the case of $Ca(H_2O)_n^{2+}$ clusters the $Ca^{2+}-O$ internuclear distance computed by using the US-PW approach is typically 0.03 Å shorter than the DNP basis set. This tendency of the US pseudopotentials to underestimate the cation−oxygen distance has been observed previously for $Al(H_2O)_n^{3+}$ clusters, where the ultrasoft pseudopotential was used to represent the inner core electrons of the cation.[34] However, as new water molecules are incorporated into the first hydration shell of Ca^{2+} the Ca−O distances computed with the US-PW and the all-electron DNP methods increase by almost the same value (see Table 1). Regarding the hydration energy ΔE of the first shell, the values computed at the PBE/US-PW level are typically 1−2 kcal/mol lower than all-electron calculations for $Ca(OH)_2(H_2O)_n$ and $Ca(HCO_3)(H_2O)_n^+$, while these differences increase to 5−8 kcal/mol in the case of $Ca(H_2O)_n^{2+}$ complexes (see the next-to-last column in Table 1). Note that a previous study on $Ca(H_2O)_n^{2+}$ clusters by Bakó et al. showed differences between norm-conserving pseudopotential-PW and all-electron results of the same order as these reported here.[6b] Moreover, if we consider the successive water binding energy, $\Delta E_{inc} = E[Ca(H_2O)_n^{2+}] - E[Ca(H_2O)_{n-1}^{2+}] - E[H_2O]$, whose values are listed in the last column of Table 1, then PBE/US-PW and PBE/DNP calculations are in much better agreement, with differences of typically 1−2 kcal/mol.

We now assess the quality of the DMol^3 PBE/DNP method, which has been used to calculate the structures and energetics of the $[Ca(HCO_3)_m(H_2O)_n]^{2-m}$ clusters. We present in Table 2 the optimized $r(Ca^{2+}-O)$ internuclear distance and hydration energy ΔE of the first solvation shell of the hexahydrated $Ca(H_2O)_6^{2+}$ complex, computed at different DFT and ab initio levels and with different basis sets. We start by considering the effect of the basis set and observe that the results obtained with the numeric DNP basis are in good agreement with the experimental value of $r(Ca^{2+}-O)$ (2.42 ± 0.05 Å[35]) and close to the calculation that employed the most accurate Gaussian basis set [the aug-cc-pVTZ for O, H and cc-pVTZ for Ca], as the $Ca^{2+}-O$ distance differs by only 0.01 Å and the water binding energy by just 0.7 kcal/mol. With regard to the numeric basis set, calculations performed with a double-numeric quality basis set (DN), and DN basis with polarization functions except for hydrogen atoms (DND), suggest that polarized functions on all atoms (DNP) are important to have convergent structural and energetic properties. Concerning the Gaussian functions, the 6-31G(d,p) basis set, which is variationally comparable to DNP, gives a first shell hydration energy that differs by 33 kcal/mol from the most accurate (aug)-cc-pVTZ basis. Moreover, note that the addition of diffuse Gaussian functions [6-31G(d,p) → 6-31++G(d,p)] is more important than increasing the basis set contraction to a triple-ζ basis [6-311G(2d,2p) or cc-pVTZ] in order to have an accurate evaluation of the binding energy ΔE.[36] Finally, we observe that single-point calculations with the (aug)-cc-pVTZ basis sets on the geometries obtained by using smaller basis sets [6-31G(d,p), 6-31++G(d,p) or DNP] have little effect on the absolute value of the binding energy.

Before considering the effect of the exchange-correlation functional, we would like to comment on the effect of the BSSE. In a previous study on doubly charged metal ion−water species, which also included Ca^{2+}, Pavolov et al.[37] showed that the dominant effect of the BSSE for these kinds of complexes is not on the total energy but on properties like the dipole moment and the polarizability of the water molecules. Therefore, because the Ca^{2+}−water interaction is mainly electrostatic, we have analyzed the BSSE by considering the effect of a *ghost* basis set (placed at the distance of the Ca^{2+} in the $Ca(H_2O)_6^{2+}$ complex) on the computed dipole moment of free water (μ_{H_2O}). The ghost basis set changed μ_{H_2O} from 2.02 to 1.92 D at the PBE/6-31++G(d,p) level, from 1.82 to 1.86 with the 6-311++G(2d,2p) basis set, and from 1.80 D to just 1.79 D when using the (aug)-cc-pVTZ basis set, a value that agrees quite well with experiment (1.85 D[38]). This led us to conclude that the (aug)-cc-pVTZ basis set could be considered BSSE free and the binding energy computed at this level practically convergent. The binding energy calculated at the PBE/6-311++G(2d,2p) and PBE/(aug)-cc-pVTZ levels differs by 1.1 kcal/mol. In Table 2, the effect of the exchange-correlation functional is also reported. The following main observations can be made: (i) The binding energy obtained at the LDA-VWN level is very inaccurate as it shows its notorious overbinding behavior. (ii) Results obtained with the HMDFT methods, mPWB1K and in particular mPW1B95, are closer to PBE/DNP values than to BLYP/DNP values. (iii) The hydration energies of first solvation shell computed at the mPW1B95/6-31++G(2d,2p) level on top of mPW1B95/6-31++G(d,p) and PBE/DNP geometries differ by only 0.1 kcal/mol. Furthermore, note that the binding energy computed at the MP2/6-311++G(2d,2p) level with use of the PBE/DNP geometries agrees very well with the mPW1B95 and PBE results. Regarding the calculations at the HF level, the $Ca^{2+}-O$ internuclear distance obtained by using the BS-HF basis set agrees well with experiment [a value of 2.44 Å has been obtained by using the standard 6-31G(d,p) for Ca] but the computed binding energy that employed the most accurate Gaussian basis set [the aug-cc-pVTZ for O, H and cc-pVTZ for Ca] is approximately 8 kcal mol^{-1} lower than MP2.

SCHEME 2: Definition of the Possible Coordination Modes of the (Bi)carbonate Ion

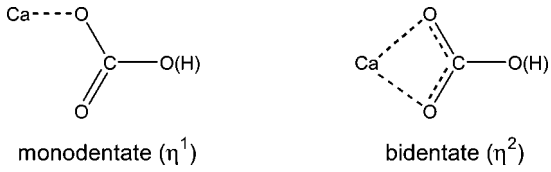

Therefore, these results suggest that calculations on the calcium−oxygen complexes can be performed to a good level of accuracy by using the computationally convenient PBE/DNP method.

B. Structural Properties in Solution: Results from the CPMD Simulations. Before discussing the structural properties of calcium (bi)carbonate in solution, we have classified in Scheme 2 the coordination mode of the (bi)carbonate ion to Ca^{2+} as monodentate (η^1) and bidentate (η^2), depending on the number of oxygen atoms directly coordinated to the cation.

In Figure 1, the time evolution of the Ca−O distance during simulation A is monitored for the oxygens of the (bi)carbonate ion (dashed lines) and for all water molecules which are considered to be part of the first solvation shell of Ca^{2+} at the beginning of the simulation (continuous lines). The criterion to define the first solvation shell of Ca^{2+} was based on the analysis of the radial distribution function of calcium−oxygen to be discussed later. Figure 2 displays a series of representative snapshots of simulation A. In the initial configuration HCO_3^- is in the second coordination sphere of Ca^{2+}, i.e., $r(Ca-O_c) \approx 4.8$ Å, with the OH^- ion placed in close proximity [Figure 2a]. Within the first picosecond HCO_3^- is involved in a H-transfer process with the hydroxide ion and with the water molecules close to HCO_3^-, so that after a short ab initio molecular dynamics run the bicarbonate is actually in its dehydrogenated form (CO_3^{2-}) [Figure 2b]. Initially, six water molecules surround the Ca^{2+} ion but at 6.9 ps the carbonate ion enters the first solvation shell of calcium [Figure 2c] and coordinates to Ca^{2+} in a monodentate mode [Figure 2d]. An intermediate state occurs during this carbonate−water exchange, where the cation−oxygen coordination number changes from 6 to 7 and the six H_2O molecules and the CO_3^{2-} form an approximately pentagonal bipyramidal structure [Figure 2d], with a lifetime of ∼0.4 ps (see Figure 1). Our simulations therefore suggest that the formation of the $CaCO_3$ monomer would occur with an associative mechanism. This result is in line with a recent CPMD study on the hydration properties of Ca^{2+},[6e] which showed that the hydration structure of calcium in water is highly variable as the 6-fold coordination is only marginally preferred over the next lowest local minimum, a 7-fold pentagonal bipyramidal configuration.[6e] At ∼7.5 ps one water leaves the first coordination shell from the axial position [red line in Figure 1 and Figure 2e] and the coordination number returns to six [Figure 2f].

Information regarding the structural properties of the dominant building block of calcium (bi)carbonate in water can be determined from pair radial distribution functions (RDFs) $g_{\alpha\beta}(r)$, which represent the probability, relative to a random distribution, of finding an atom of type β at a distance r from an atom of type α. To calculate the RDFs, starting from the last snapshot of simulation A (Figure 1) (which consisted of 53 water molecules and one $CaCO_3$ unit) the coefficients of the electron wave function were reoptimized and after an equilibration of 2 ps the statistics were collected for an additional 20 ps. Moreover,

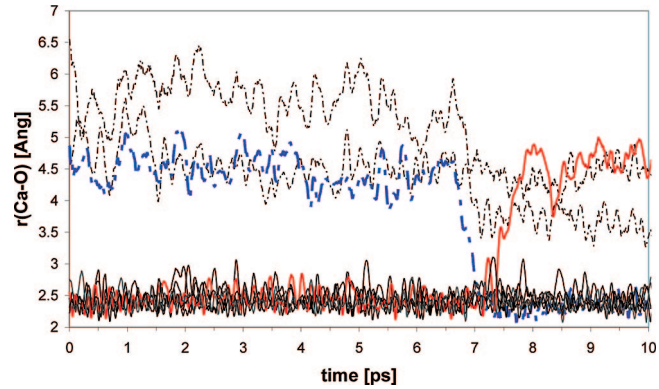

Figure 1. Time evolution of Ca−O distance during simulation A. The solid black lines represent oxygens of the water molecules that are part of the first hydration shell of Ca^{2+} at the beginning of the simulation, and the dashed lines represent the oxygens of the (bi)carbonate ion.

to study the structure of the protonated species $CaHCO_3^+$, starting from the last configuration shown in Figure 2f, $CaCO_3$ was replaced by $CaHCO_3^+$ (simulation B, which therefore consisted of 52 water molecules and one unit of $CaHCO_3$), and after 2 ps of equilibration the statistics were collected for an additional 11 ps.

Figure 3 displays the RDFs of the Ca−O and Ca−H pairs obtained in simulations A and B. For both species, the first peaks of $g_{CaO}(r)$ and $g_{CaH}(r)$ are centered at approximately 2.36 and 3.0 Å, respectively. In Figure 3 we also show the running integration number, $n_{CaX}(r) = \{4\pi N/V\}\int_o^r g_{CaX}(r')\,dr'$, where N is the number of oxygen or hydrogen atoms, V is the volume of the simulation cell, and X represents oxygen or hydrogen atoms. The value of $n_{CaO}(r)$ at the first minimum of $g_{CaO}(r)$ (r = 3.1 Å) gives the average number of oxygen atoms which are part of the first coordination shell of calcium and this is 6.3 for both simulations A and B. These values include oxygens of the water and (bi)carbonate molecules. However, to obtain the hydration number of the calcium (bi)carbonate in water, i.e., the number of water molecules which are part of the $Ca(H)CO_3$ monomer, it is necessary to consider the contribution of the water oxygens (O_w) to the Ca−O radial distribution function alone [$g_{CaOw}(r)$]. In the same way, to determine the dominant coordination mode of the (bi)carbonate to the calcium ion, we have to consider only the oxygens of the (bi)carbonate ion [$g_{CaOc}(r)$].

In Figure 3c, the $g_{CaOw}(r)$ from simulation A and simulation B are compared to the Ca−O RDF of a calcium ion in water, which has been obtained from a CPMD simulation of Ca^{2+} with 53 water molecules, where 2 ps of equilibration were followed by 11 ps of production time. For Ca^{2+} in water the running coordination number at the first minimum of $g_{CaOw}(r)$ indicates that the first solvation shell around the ion is 6 water molecules, a result fully consistent with previous CPMD simulations of calcium in water, where larger number of water molecules were employed [1 Ca^{2+} in 54 H_2O in ref 6b; 1 Ca^{2+} in 60 H_2O in ref 6d; 1 Ca^{2+} in 63 H_2O in ref 6e]. On the basis of this result, we do not expect significant errors in the determination of the first hydration shell of Ca^{2+} in the calcium (bi)carbonate monomer. Moreover, a study on Al^{3+} in 32 and 62 water molecules[34] showed that there are negligible differences in the structure of the first solvation shell between the two simulations and appreciable differences are observed only for the second hydration shell. For Ca^{2+} the first maximum in the RDF is located at 2.35 Å, approximately 0.05−0.1 shorter than previously reported, which could be explained in terms of the tendency of the US pseudopotential to slightly underestimate

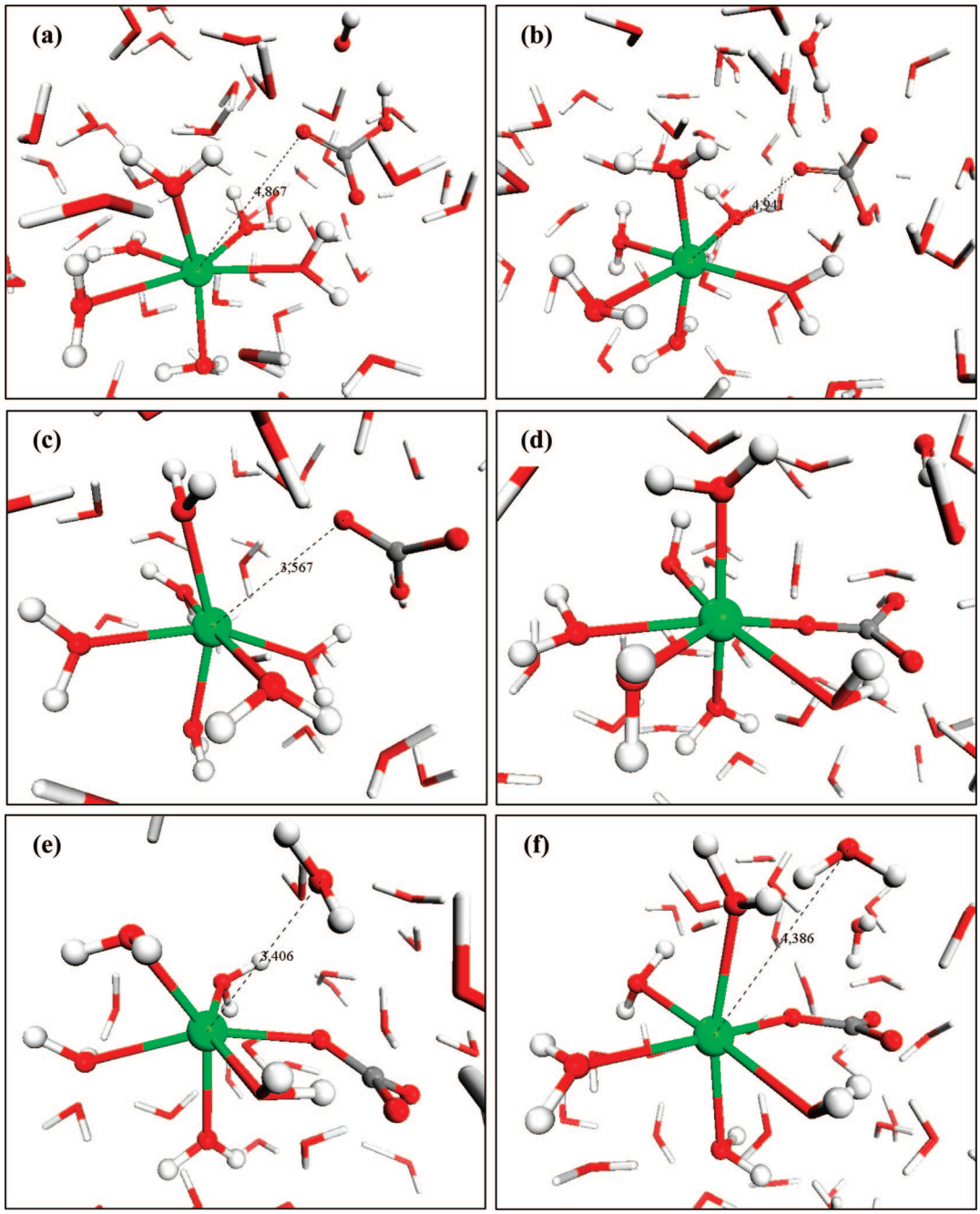

Figure 2. Representative snapshots from the CPMD simulation A taken at $t = 0$ (a), 1 (b), 6.9 (c), 7.2 (d), 7.5 (e), and 10 ps (f).

the $Ca^{2+}-O$ distance, as discussed in Section IIIA. For $CaCO_3$ in water (simulation A), the first peak of $g_{CaOw}(r)$ is less structured and slightly shifted to higher Ca−O distances (2.38 Å) compared to Ca^{2+}, while the running coordination number $n_{CaOw}(r)$ is characterized by a less clear plateau in the running coordination number $n_{CaOw}(r)$. The average number of water molecules in the first coordination shell of calcium at the first minimum of $g_{CaOw}(r)$ ($r = 3.1$ Å) gives a water coordination number of 5.2 for $Ca-O_w$ in simulation A. For $CaHCO_3$ (simulation B), the first peak of $g_{CaOw}(r)$ is centered at 2.36 Å and the running coordination number at the first minimum of $g_{CaOw}(r)$ ($r = 3.2$ Å) also gives a water coordination number of 5.2. There results indicate that the monomer of $CaCO_3$ in aqueous solution has, on average, five water molecules in the first solvation shell of Ca^{2+}.

Figure 3d displays the calcium−oxygen (bi)carbonate RDF. For $CaCO_3$ (simulation A) the first peak of $g_{CaOc}(r)$ is centered at 2.30 Å (0.08 Å shorter than the average $Ca-O_w$ distance) while the value of the running coordination number $n_{CaO}(r)$ at the first minimum of $g_{CaOc}(r)$ (~3.2 Å) is 1.1, which indicates that the most stable coordination mode for CO_3^{2-} is the monodentate. In the case of $CaHCO_3^+$ (simulation B) the profile of the $g_{CaOc}(r)$ is more irregular than the one obtained from simulation A, probably because the statistics in this case have been collected for a shorter simulation period. However, if we consider that $n_{CaOc}(r) \leq 1.5$ indicates a preference for the η^1-coordination mode, then a value for the running coordination number of 1.5 is obtained only at $r(Ca-O) = 3.5$ Å, suggesting that the most stable coordination for HCO_3^- is also the η^1-coordination.

Therefore, our CPMD simulations indicate that the dominant building block (monomer) of calcium carbonate and calcium bicarbonate in aqueous solution is $Ca[\eta^1\text{-}(H)CO_3](H_2O)_5$, i.e,. the preferred hydration number is five, which is the same value

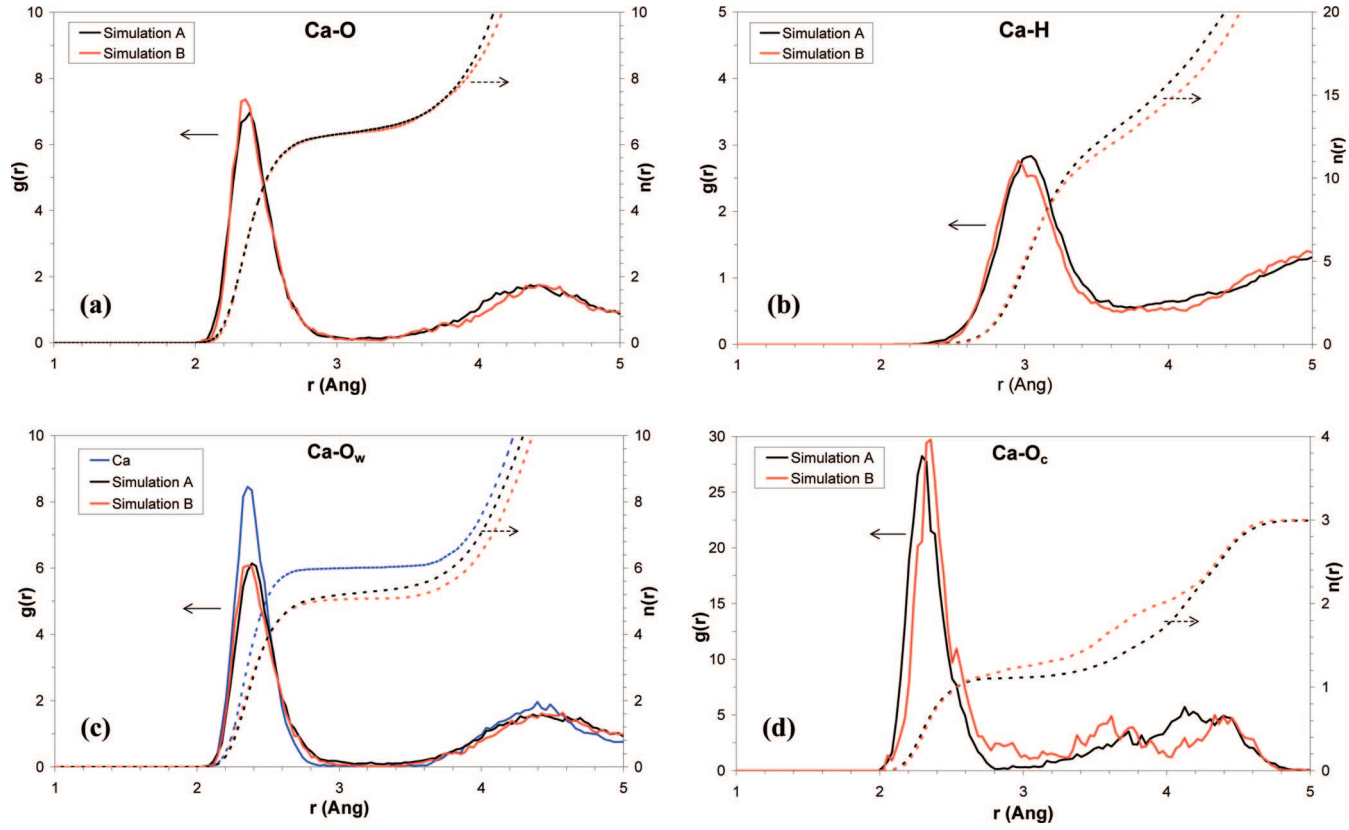

Figure 3. Ca−O, Ca−H, Ca−O_w, and Ca−O_c radial distribution functions and running coordination numbers obtained in simulations A and B.

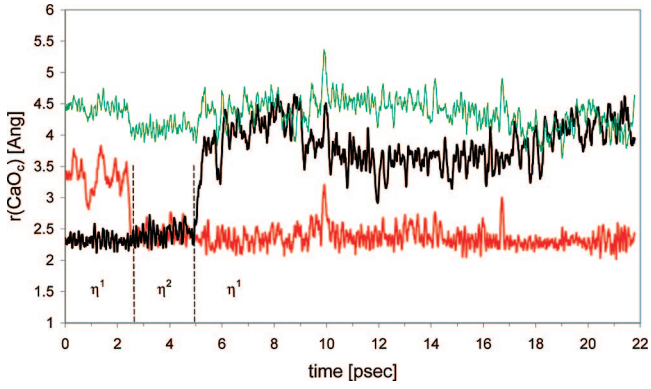

Figure 4. Time evolution of Ca−O distance during simulation A for the oxygens of the carbonate ion. The vertical dashed lines denote a change between the monodentate (η^1) and bidentate (η^2) coordination mode.

obtained in the recent classical MD study on $CaCO_3$ in water,[7] while the (bi)carbonate coordinates the calcium in a monodentate mode.

Finally, it is interesting to consider in Figure 4 the variation of Ca−O carbonate distance as a function of time for the oxygens of the carbonate ion (simulation A). We note that during the 22 ps of dynamics there is an exchange of the oxygens directly coordinated to calcium in a monodentate (η^1) mode. This exchange occurs via an intermediate state where the carbonate ion is η^2-coordinated to Ca^{2+} and this intermediate is characterized by a lifetime of approximately 2.5 ps (see Figure 4). Moreover, the analysis of the time evolution of the r(Ca−O_c) distance in Figure 4 reinforces our hypothesis that the η^1-coordination is actually the most stable coordination mode for the (bi)carbonate ion, but also that the interconversion between the η^1- and η^2-coordination modes is actually quite facile.

A similar analysis for simulations C and D (available in the Supporting Information) confirms that the dominant coordination mode of the (bi)carbonate ion and number of water molecules in the first solvation shell of Ca^{2+} is η^1 and five, respectively, and shows that during the 10 ps of dynamics there is a change in the coordination mode of the type $\eta^1 \rightarrow \eta^2$ (with a lifetime of ∼2 ps) $\rightarrow \eta^1$ (with a lifetime of 10 ps).

A final remark concerns the use of 400 K as the temperature at which all the CPMD simulations have been performed. In the oxygen−oxygen radial distribution functions obtained from simulations A−D (available in the Supporting Information) the peak corresponding to the O_w−O_w pairs is located at ∼2.7 Å and characterized by a height of ∼2.5 density units, which is in very good agreement with the values obtained from extensive CPMD (PBE) simulations on water by Sit et al.[19] at the same temperature and comparable with the experimental value of 2.80 Å and 2.75 at 300 K.[39]

C. Speciation in Aqueous Calcium Bicarbonate: Results from DFT Hybrid Microsolvation/Continuum Simulations. The different thermodynamic energies of the calcium bicarbonate $[Ca(HCO_3)_m(H_2O)_n]^{2-m}$ $[Ca(HCO_3)_m(H_2O)_n{}^{2-m}$, $m = 0-3$ $n = 1-6]$ complexes as calculated from the microsolvation model are listed in Table 3. For Ca^{2+}, the free energy of hydration of the first shell ($\Delta G_{clust} = -183.6$ kcal mol^{-1}) is considerably less than the experimental value (−381 kcal mol^{-1} [40]), suggesting a large contribution from the bulk beyond the first hydration shell. For calcium, however, the number of nearest water molecules is highly variable, with reported values ranging from 5.5 to 10.0.[35] Thus, to assess the PBE/DNP-COSMO method used here to compute the hydration free energy within the microsolvation/continuum approach, we have also considered the case of Mg^{2+} in water, which is characterized by an unambiguous 6-fold coordinated water environment.[6e,41] Therefore, we note in Table 3 that the computed first shell free

TABLE 3: Thermodynamic Data for Gas-Phase Clustering Processes of the $[Ca(HCO_3)_m(H_2O)_n]^{2-m}$ Species As Computed at the PBE/DNP Level of Theory[a]

species	ΔE	ΔH_{clust}	ΔG_{clust}
$Mg(H_2O)_6^{2+}$	−321.1	−338.91	−262.4
$Ca(H_2O)_6^{2+}$	−245.3	−236.0	−183.6
$Ca(\eta^2\text{-}HCO_3)(H_2O)^+$	−31.0	−29.5	−20.8
$Ca(\eta^2\text{-}HCO_3)(H_2O)_2^+$	−59.9	−56.6	−39.0
$Ca(\eta^2\text{-}HCO_3)(H_2O)_3^+$	−85.2	−80.5	−54.3
$Ca(\eta^1\text{-}HCO_3)(H_2O)_3^+$	−81.0	−77.9	−48.2
$Ca(\eta^2\text{-}HCO_3)(H_2O)_4^+$	−105.3	−99.1	−62.8
$Ca(\eta^1\text{-}HCO_3)(H_2O)_4^+$	−104.3	−98.9	−62.0
$Ca(\eta^2\text{-}HCO_3)(H_2O)_5^+$	−123.2	−115.5	−69.4
$Ca(\eta^1\text{-}HCO_3)(H_2O)_5^+$	−123.6	−116.5	−69.6
$Ca(\eta^1\text{-}HCO_3)(H_2O)_6^+$	−138.6	−129.2	−70.5
$Ca(HCO_3)_2(H_2O)$	−18.3	−16.7	−7.3
$Ca(HCO_3)_2(H_2O)_2$	−33.3	−30.3	−12.1
$Ca(HCO_3)_2(H_2O)_3$	−44.1	−40.4	−10.3
$Ca(HCO_3)_2(H_2O)_4$	−61.2	−55.0	−15.4
$Ca(HCO_3)_3(H_2O)^-$	−10.5	−8.9	0.2
$Ca(HCO_3)_3(H_2O)_2^-$	−29.2	−26.2	−5.4
$Ca(HCO_3)_3(H_2O)_3^-$	−39.5	−16.1	23.0

[a] Values in kcal mol^{-1}.

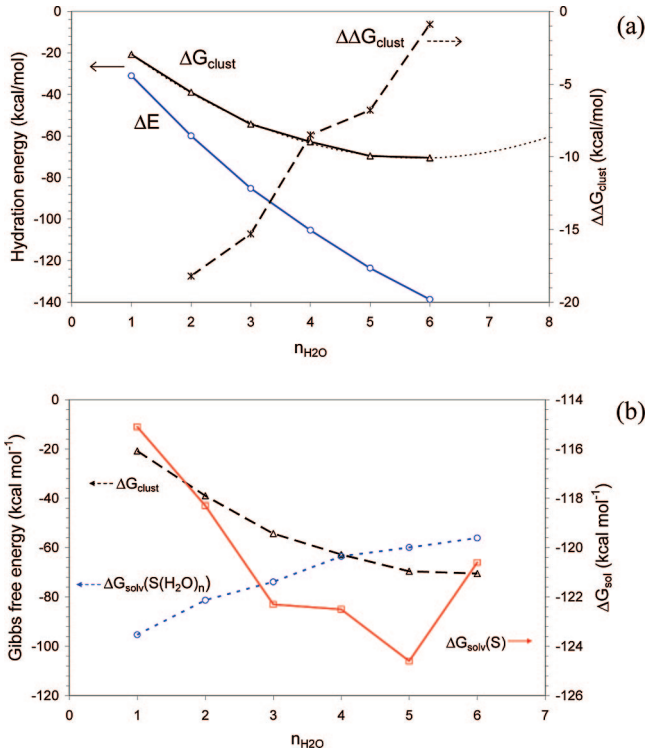

Figure 5. (a) Hydration energy, ΔE, hydration free energy, ΔG_{clust}, of the first solvation shell, and $\Delta\Delta G_{clust} = \Delta G_{n+1} - \Delta G_n$, as a function of the hydration number n_{H_2O} for the species $[Ca(HCO_3)(H_2O)_n]^+$. (b) Variation of the hydration free energy of the first solvation shell, ΔG_{clust}, free energy of solvation, $\Delta G_{solv}(S(H_2O)_n)$, and total hydration free energy, $\Delta G_{solv}(S)$, as a function of the hydration number n_{H_2O} for the species $[Ca(HCO_3)(H_2O)_n]^+$.

energy of Mg^{2+} ($\Delta G_{clust} = -283.6$ kcal mol^{-1}) is also considerably lower than the experimental hydration free energy (−455.5 kcal mol^{-1}[40]), which reinforces the above statement that the contribution beyond the first solvation shell is important. For all species considered in Table 3 the change in the energy value when going from ΔE to ΔG_{clust} is quite large and increases

TABLE 4: Calculated Solvation Free Energy of Mg^{2+}, Ca^{2+}, and $Ca(HCO_3)_m^{2-m}$ As Computed at the PBE/DNP-COSMO Level[a]

species	$n\Delta G_{vap}$ (H_2O)	ΔG_{clust}	ΔG^*_{solv} ($S(H_2O)_n$)	$\Delta G^*_{solv}(S)$
$Mg(H_2O)_6^{2+}$	6.0	−262.4	−182.4	−438.8
$Ca(H_2O)_6^{2+}$	6.0	−183.6	−175.1	−352.7
$Ca(\eta^2\text{-}HCO_3)^+$			−111.4	−111.4
$Ca(\eta^2\text{-}HCO_3)(H_2O)^+$	1.0	−20.8	−95.3	−115.1
$Ca(\eta^2\text{-}HCO_3)(H_2O)_2^+$	2.0	−39.0	−81.3	−118.3
$Ca(\eta^2\text{-}HCO_3)(H_2O)_3^+$	3.0	−54.3	−69.5	−120.8
$Ca(\eta^1\text{-}HCO_3)(H_2O)_3^+$	3.0	−48.2	−73.9	−122.3
$Ca(\eta^2\text{-}HCO_3)(H_2O)_4^+$	4.0	−62.8	−63.5	−122.3
$Ca(\eta^1\text{-}HCO_3)(H_2O)_4^+$	4.0	−62.0	−64.5	−122.5
$Ca(\eta^2\text{-}HCO_3)(H_2O)_5^+$	5.0	−69.4	−59.0	−123.4
$Ca(\eta^1\text{-}HCO_3)(H_2O)_5^+$	5.0	−69.6	−59.9	−124.6
$Ca(\eta^1\text{-}HCO_3)(H_2O)_6^+$	6.0	−70.5	−56.1	−120.6
$Ca(HCO_3)_2$			−31.8	−31.8
$Ca(HCO_3)_2(H_2O)$	1.0	−7.3	−25.8	−32.2
$Ca(HCO_3)_2(H_2O)_2$	2.0	−12.1	−24.7	−33.1
$Ca(HCO_3)_2(H_2O)_3$	3.0	−10.3	−25.8	−33.1
$Ca(HCO_3)_2(H_2O)_4$	4.0	−15.4	−23.7	−35.1
$Ca(HCO_3)_3^-$			−58.6	−58.6
$Ca(HCO_3)_3(H_2O)^-$	1.0	0.2	−58.6	−57.4
$Ca(HCO_3)_3(H_2O)_2^-$	2.0	−5.4	−58.4	−61.8
$Ca(HCO_3)_3(H_2O)_3^-$	3.0	23.0	−61.5	−35.5

[a] Values in kcal mol^{-1}.

with the number of water molecules coordinated to calcium because most of this quantity is due to entropy, which decreases with the formation of the cluster. The variation in the calculated hydration energy of the first shell, ΔE, and hydration free energy of the first shell, ΔG_{clust}, of the $Ca(HCO_3)(H_2O)_n^+$ species as a function of the hydration number n is displayed in Figure 5a. In this figure, for a certain hydration number n the energy of the most stable isomer has been reported when both η^1 and η^2 coordination modes were located as minimum structures. Note that no optimized structure could be found for $n = 7$, i.e., where seven water molecules are directly coordinated to calcium. The computed values of ΔE decrease almost linearly with n. On the other hand, the values of the hydration free energy are well fitted by using a second order polynomial (the dotted black line), with $\Delta G_{clust}(n = 6)$ representing the minimum of the parabola. Similarly, if we consider the plot of $\Delta\Delta G_{clust}$, defined as $\Delta\Delta G_{clust} = \Delta G_{n+1} - \Delta G_n$, then the variation of the Gibbs free energy necessary to add the hypothetical seventh water molecule to the $Ca(\eta^1\text{-}HCO_3)(H_2O)_6^+$ cluster is positive, meaning that this process is thermodynamically not favorable. More importantly, the computed energies reported in Figure 5a highlight the importance of including thermal corrections and the entropic terms to obtain a correct description of the stability of calcium bicarbonate species. Note that the 7-fold coordinated $Ca(\eta^1\text{-}HCO_3)(H_2O)_6^+$ is predicted to be slightly more stable (about 1 kcal mol^{-1}) than the 6-fold $Ca(HCO_3)(H_2O)_5^+$ species within the microsolvation model, in disagreement with the result obtained from the CPMD simulations.

Previous studies on divalent ions including Ca^{2+} and Mg^{2+} have shown that bulk solvent effects are quite important to obtain a realistic description on the solvation energies of these metallic cations.[42] The free energies of solvation $\Delta G^*_{solv}(S(H_2O)_n)$ obtained from the COSMO model are listed in Table 4. The predicted solvation free energy of Mg^{2+} obtained by using eq 1 (−438.8 kcal mol^{-1}) now is in good agreement with the experimental value (−455.5 kcal/mol).[40] Therefore, a more

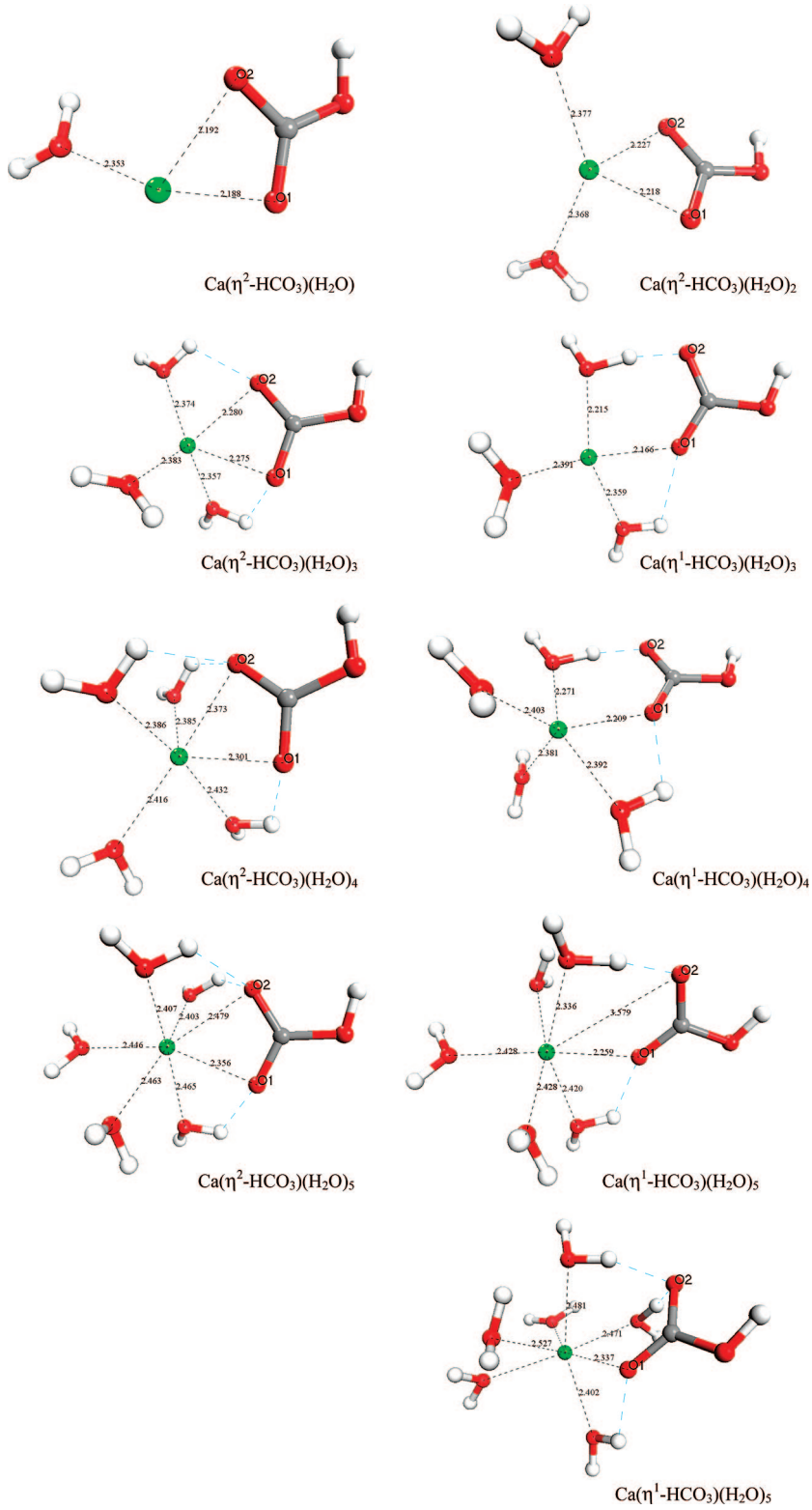

Figure 6. Optimized structures of the $Ca(HCO_3)(H_2O)_n$ clusters, $n = 1-6$, as computed at the PBE/DNP level. Bond lenghts in angstroms.

realistic prediction of the solvation free energies of the calcium bicarbonate species may be obtained by using the discrete-continuum model.

The combination of the discrete, ΔG_{clust}, and the continuum, $\Delta G_{solv}(S(H_2O)_n)$, contributions to the free energy of solvation allows a way to determine the most stable first shell of coordination of calcium bicarbonate in aqueous solution.[12] Figure 5b displays the variation of the hydration free energy of the first shell (ΔG_{clust}), free energy of solvation [ΔG_{solv}-($S(H_2O)_n$)], and total hydration free energy [$\Delta G_{solv}(S)$] of the $Ca(HCO_3)(H_2O)_n^+$ species as a function of the hydration number n. For $n = 3$, 4, and 5, where both the monodentate (η^1) and the bidentate (η^2) coordination modes were located as local minima, the energy values of the most stable isomer are reported. Due to the opposite trend of the discrete and continuum contributions with the hydration number n, an optimum value is found as a compromise between ΔG_{clust} and $\Delta G_{solv}(S(H_2O)_n)$ at $n = 5$, which corresponds to the species Ca(η^1-HCO_3)-

TABLE 5: Optimized Structure (distances in Å and angles in deg) of $Ca(HCO_3)_m(H_2O)_n$ Clusters As Computed at the PBE/DNP Level[a]

species	$r(Ca-O_1)$	$r(Ca-O_2)$	$r(Ca-OH)$	$\theta(O_1-C-O_2)$	$r(Ca-O_w)$
$Ca(\eta^2\text{-}HCO_3)(H_2O)^+$	2.19	2.19	3.85	120.7	2.35
$Ca(\eta^2\text{-}HCO_3)(H_2O)_2^+$	2.22	2.23	3.88	121.5	2.30
$Ca(\eta^2\text{-}HCO_3)(H_2O)_3^+$	2.28	2.28	3.94	121.9	2.37
$Ca(\eta^1\text{-}HCO_3)(H_2O)_3^+$	2.17	3.44	4.33	125.6	2.32
$Ca(\eta^2\text{-}HCO_3)(H_2O)_4^+$	2.30	3.37	4.01	122.5	2.40
$Ca(\eta^1\text{-}HCO_3)(H_2O)_4^+$	2.21	3.52	4.39	125.7	2.36
$Ca(\eta^2\text{-}HCO_3)(H_2O)_5^+$	2.36	2.48	4.10	122.9	2.44
$Ca(\eta^1\text{-}HCO_3)(H_2O)_5^+$	2.26	3.58	4.44	125.9	2.41
$Ca(\eta^1\text{-}HCO_3)(H_2O)_6^+$	2.34	3.43	4.46	125.4	2.46

[a] The oxygen from water molecules is labeled O_w.

$(H_2O)_5^+$. Therefore, according to the microsolvation/continuum approach the most stable $Ca(HCO_3)^+$ species in aqueous solution has five water molecules in the first coordination sphere of calcium, while the bicarbonate ion is η^1-coordinated to Ca^{2+}. This result agrees with the Car−Parrinello simulations reported in Section IIIB. However, our values of the solvation free energies suggest that $Ca(\eta^1\text{-}HCO_3)(H_2O)_5^+$ is thermodynamically more stable by just 1 kcal mol^{-1} than its isomer $Ca(\eta^2\text{-}HCO_3)(H_2O)_5^+$, which could reflect the facile interconversion observed between η^1 and the η^2 coordinated species observed during the CPMD simulation (see Figure 4). Moreover, the $Ca(\eta^1\text{-}HCO_3)(H_2O)_5^+$ complex is only 3−4 kcal mol^{-1} more stable than the $CaHCO_3^+$ complexes where 3, 4, and 6 water molecules are explicitly considered (see Table 4). These small differences in the free energy of solvation reflect the highly variable hydration number of Ca^{2+} in aqueous solution.

With regard to the $Ca(HCO_3)_2$ and $Ca(HCO_3)_3^-$ species, the computed total free energies of solvation, $\Delta G_{solv}(S)$, listed in Table 4 suggest that these calcium bicarbonates can exist in aqueous solution, that $Ca(HCO_3)_2(H_2O)_4$ is preferred over $Ca(HCO_3)_2(H_2O)$, $Ca(HCO_3)_2(H_2O)_2$, and $Ca(HCO_3)_2(H_2O)_3$, and that $Ca(HCO_3)_3(H_2O)_2^-$ is more stable than the $Ca(HCO_3)_3(H_2O)^-$ and $Ca(HCO_3)_3(H_2O)_3^-$ species. The values of $\Delta G_{solv}(S)$ for these species also suggest that the number of water molecules directly coordinated to $Ca(HCO_3)_2$ and $Ca(HCO_3)_3$ in aqueous solution is highly variable. Moreover, these results indicate that the process of calcium carbonate nucleation from aqueous solution could take place not just as an attachment of single $CaHCO_3^+$ building units, but also in an aggregation process involving species like $Ca(HCO_3)_2$ and $Ca(HCO_3)_3$.

The predicted structures of $Ca(HCO_3)(H_2O)_n$, $n = 1-6$, clusters are given in Figure 6 and summarized in Table 5. For $n = 1$, 2 the bicarbonate was only found in the bidentate η^2-coordination to calcium, while for $n = 6$ the optimized geometry has only the HCO_3^- in the η^1-coordination. The other hydrated species ($n = 3-5$) have both coordination modes as local minima. Table 5 shows that O1, the oxygen of the bicarbonate in the "trans" position with the H atom, is always more strongly coordinated to the calcium than O2, the oxygen in the "cis" position. Furthermore, as n increases so does the internuclear distance $r(Ca-O_1)$ [from 2.17 Å in $Ca(\eta^1\text{-}HCO_3)(H_2O)_3^+$ to 2.34 Å $Ca(\eta^1\text{-}HCO_3)(H_2O)_6^+$] and the average value of the calcium−water distance $r(Ca-O_w)$ [from 2.32 Å in $Ca(\eta^1\text{-}HCO_3)(H_2O)_3$ to 2.46 Å in $Ca(\eta^1\text{-}HCO_3)(H_2O)_6^+$]. This trend could explain why a minimum energy structure has not been located for $n = 7$, as the coordination space of Ca^{2+} in the hetero-ion $CaHCO_3^+$ can be considered "saturated" when the hydration number of the first shell reaches the value $n = 6$.

IV. Conclusion

This study has reported static and dynamic DFT-PBE calculations on calcium (bi)carbonate species in water in order to examine the structure and the hydration environment of the building blocks of $CaCO_3$ in aqueous solution.

Car−Parrinello molecular dynamics simulations were performed on simulation cells where the calcium carbonate and calcium bicarbonate species were considered in combination with 52 water molecules. The results from these calculations suggest that the formation of the monomer of $CaCO_3$ occurs with an associative mechanism and that the dominant building block of calcium (bi)carbonate in aqueous solution is $Ca[\eta^1\text{-}(H)CO_3](H_2O)_5$, i.e., the preferred hydration number is five, while the (bi)carbonate is coordinated to the calcium in a monodentate mode. However, the analysis of the calcium−oxygen time evolution indicates that the interconversion between the η^1- and η^2-coordination modes is quite facile.

Static DFT-PBE calculations using a hybrid microsolvation/continuum approach to determine the structure and stability of $[Ca(HCO_3)_m(H_2O)_n]^{2-m}$ species in aqueous solution have also been conducted. In agreement with the CPMD simulations, the discrete-continuum approach indicates that the $Ca[\eta^1\text{-}HCO_3](H_2O)_5$ species is the most stable calcium bicarbonate species in solution. Moreover, the computed hydration free energies of the species $[Ca(HCO_3)_m(H_2O)_n]^{2-m}$ suggest that the thermodynamic stability of the η^1-coordinated species compared with η^2 is small, approximately 1 kcal mol^{-1}, which could reflect the facile interconversion observed between the η^1 and η^2 coordinated species during the ab initio molecular dynamics. Finally, the hybrid microsolvation/continuum calculations further predict the $Ca(HCO_3)_2$ and $Ca(HCO_3)_3^-$ species to occur in an aqueous environment as $Ca(HCO_3)_2(H_2O)_4$ and $Ca(HCO_3)_3(H_2O)_2^-$, respectively.

Acknowledgment. We acknowledge the EU-funded "Mineral Nucleation and Growth Kinetics (MIN-GRO) Marie-Curie Research and Training Network" for funding (grant MRTN-CT-2006-035488). Computer resources on the UK "HPCx service" were provided via our membership of the UK's HPC Materials Chemistry Consortium (grant no. EPSRC EP/D504872). Additional computer resources were provided by the Mott-2 facilities provided via our membership of the Minerals and Ceramics Consortium (grant no. EPSRC GR/S84415). Dr. A. Tilocca is acknowledged for useful discussions.

Supporting Information Available: Ca−O, Ca−O_w, and Ca−O_c radial distribution functions and running coordination numbers obtained in simulations C and D, and O−O radial distribution functions obtained in simulations A−D. This

material is available free of charge via the Internet at http://pubs.acs.org.

References and Notes

(1) Lerman, A.; Mackenzie, F. T. *Aquat. Geochem.* **2005**, *11*, 345.

(2) (a) Bolze, J.; Peng, B.; Dingenouts, N.; Panine, P.; Naarayanan, T.; Ballauff, N. *Langmuir* **2002**, *18*, 8364. (b) Pontoni, D.; Bolze, J.; Dingenouts, N.; Naarayanan, T.; Ballauff, M. *J. Phys. Chem. B* **2003**, *107*, 5123. (c) Addadi, L.; Raz, S.; Weiner, S. *Adv. Mater.* **2003**, *15*, 959. (d) Shen, Q.; Wei, H.; Zhou, Y.; Huang, Y.; Wang, D.; Xu, D. *J. Phys. Chem. B* **2006**, *110*, 2994.

(3) (a) Duffy, D. M.; Harding, J. H. *J. Mater. Chem.* **2002**, *12*, 3419. (b) Duffy, D. M.; Harding, J. H. *Surf. Sci.* **2005**, *595*, 151.

(4) (a) Parker, S. C.; Kelsey, E. T.; Oliver, P. M.; Titiloye, J. O. *Faraday Discuss.* **1993**, *94*, 75. (b) Nygren, M. A.; Gay, D. H.; Catlow, C. R. A.; Rohl, A. L.; Wilson, M. P. *J. Chem. Soc., Faraday Trans.* **1998**, *94*, 3685. (c) Ojo, S. A.; Slater, B.; Catlow, C. R. A. *Mol. Simul.* **2002**, *28*, 591.

(5) de Leeuw, N. H.; Cooper, T. G. *Cryst. Growth Des.* **2004**, *4*, 123.

(6) (a) Schwenk, C. F.; Loeffler, H. H.; Rode, B. M. *Chem. Phys. Lett.* **2001**, *349*, 99. (b) Bakó, I.; Hutter, J.; Pálinkás, G. *J. Chem. Phys.* **2001**, *115*, 9838. (c) Naor, M. M.; van Nostrand, K.; Dellago, C. *Chem. Phys. Lett.* **2003**, *369*, 159. (d) Lighstone, F. C.; Schwegler, E.; Allesh, M.; Gygi, F.; Galli, G. *ChemPhysChem* **2005**, *6*, 1745. (e) Ikeda, T.; Boero, M.; Terakura, K. *J. Chem. Phys.* **2007**, *127*, 74503.

(7) Bruneval, F.; Donadio, D.; Parrinello, M. *J. Phys. Chem. B* **2007**, *111*, 12219.

(8) Morse J. W.; Mackenzie, F. T. Geochemistry of sedimentary carbonates. In *Developments in Sedimentology*; Elsevier: Amsterdam, The Netherlands, 1990; Vol. *48*.

(9) (a) Mora-Fonz, M. J.; Catlow, C. R. A.; Lewis, D. W. *Angew. Chem., Int. Ed.* **2005**, *44*, 3082. (b) Mora-Fonz, M. J.; Catlow, C. R. A.; Lewis, D. W. *J. Phys. Chem. C* **2007**, *111*, 18155.

(10) Tossell, J. A. *Geochem. Cosmochim. Acta* **2005**, *69*, 283.

(11) Car, R.; Parrinello, M. *Phys. Rev. Lett.* **1985**, *55*, 2471.

(12) Pliego, J. R.; Riveros, J. M. *J. Phys. Chem. A* **2001**, *105*, 7241.

(13) Quantum-ESPRESSO is a community project for high-quality quantum-simulation software, based on density-functional theory, and coordinated by Paolo Giannozzi. See http://www.quantum-espresso.org and http://www.pwscf.org.

(14) Perdew, J. P.; Burke, K.; Ernzerhof, M. *Phys. Rev. Lett.* **1996**, *77*, 3865.

(15) (a) Vanderbilt, D. *Phys. Rev. B* **1990**, *41*, 7892. (b) Laasonen, K.; Pasquarello, A.; Lee, C.; Car, R.; Vanderbilt, D. *Phys. Rev. B* **1993**, *47*, 10142.

(16) Tilocca, A.; de Leeuw, N. H. *J. Mater. Chem.* **2006**, *16*, 1950.

(17) Grossman, J. C.; Schwegler, E.; Draeger, E. W.; Gygi, F.; Galli, G. *J. Chem. Phys.* **2004**, *120*, 2004.

(18) Schwegler, E.; Grossman, J. C.; Gygi, F.; Galli, G. *J. Chem. Phys.* **2004**, *121*, 5400.

(19) Sit, P. H.-L.; Marzari, N. *J. Chem. Phys.* **2005**, *122*, 204510.

(20) (a) Fernández-Serra, M. V.; Artacho, E. *J. Chem. Phys.* **2004**, *121*, 11136. (b) VandeVondele, J.; Mohamed, F.; Krack, M.; Hunter, J.; Sprik, M.; Parrinello, M. *J. Chem. Phys.* **2005**, *122*, 14515.

(21) (a) Delley, B. *J. Chem. Phys.* **1990**, *92*, 508. (b) Delley, B. *J. Chem. Phys.* **2000**, *113*, 7756.

(22) *DMol*^{3}, Materials Studio version 4.0 from Accelrys: http://www.accelrys.com/products/mstudio/.

(23) (a) Klamt, A.; Shuurmann, G. *J. Chem. Soc., Perkin Trans.* **1993**, *2*, 799. (b) Klamt, A. *J. Phys. Chem.* **1995**, *99*, 2224.

(24) Andzelm, J.; Kölmel, C.; Klamt, A. *J. Chem. Phys.* **1995**, *103*, 9312.

(25) Klamt, A.; Jonas, V.; Bürger, T.; Lohrenz, J. C. W. *J. Phys. Chem. A* **1998**, *102*, 5074.

(26) Vosko, S. J.; Wilk, L.; Nusair, M. *Can. J. Phys.* **1980**, *58*, 1200.

(27) (a) Becke, A. D. *J. Chem. Phys.* **1988**, *88*, 2547. (b) Lee, C.; Yang, W.; Parr, R. G. *Phys. Rev. B* **1988**, *37*, 786.

(28) Frisch, M. J.; Trucks, G. W.; Schlegel, H. B.; Scuseria, G. E.; Robb, M. A.; Cheeseman, J. R.; Montgomery, J. A., Jr.; Vreven, T.; Kudin, K. N.; Burant, J. C.; Millam, J. M.; Iyengar, S. S.; Tomasi, J.; Barone, V.; Mennucci, B.; Cossi, M.; Scalmani, G.; Rega, N.; Petersson, G. A.; Nakatsuji, H.; Hada, M.; Ehara, M.; Toyota, K.; Fukuda, R.; Hasegawa, J.; Ishida, M.; Nakajima, T.; Honda, Y.; Kitao, O.; Nakai, H.; Klene, M.; Li, X.; Knox, J. E.; Hratchian, H. P.; Cross, J. B.; Adamo, C.; Jaramillo, J.; Gomperts, R.; Stratmann, R. E.; Yazyev, O.; Austin, A. J.; Cammi, R.; Pomelli, C.; Ochterski, J. W.; Ayala, P. Y.; Morokuma, K.; Voth, G. A.; Salvador, P.; Dannenberg, J. J.; Zakrzewski, V. G.; Dapprich, S.; Daniels, A. D.; Strain, M. C.; Farkas, O.; Malick, D. K.; Rabuck, A. D.; Raghavachari, K.; Foresman, J. B.; Ortiz, J. V.; Cui, Q.; Baboul, A. G.; Clifford, S.; Cioslowski, J.; Stefanov, B. B.; Liu, G.; Liashenko, A.; Piskorz, P.; Komaromi, I.; Martin, R. L.; Fox, D. J.; Keith, T.; Al-Laham, M. A.; Peng, C. Y.; Nanayakkara, A.; Challacombe, M.; Gill, P. M. W.; Johnson, B.; Chen, W.; Wong, M. W.; Gonzalez, C.; Pople, J. A. *Gaussian 3*; Gaussian, Inc.: Wallingford, CT, 2004.

(29) Basis Set Exchange: A Community Database for Computational Sciences, Schuchardt, K. L., Didier, B. T., Elsethagen, T., Sun, L., Gurumoorthi, V., Chase, J., Li, J., Windus, T. L. J. Chem. Inf. Model. **2007**. 10.1021/ci600510j. https://bse.pnl.gov/bse/portal.

(30) Zhao, Y.; Truhlar, D. G. *J. Phys. Chem. A* **2004**, *108*, 6908.

(31) Zhao, Y.; Truhlar, D. G. *J. Phys. Chem. A* **2005**, *109*, 5656.

(32) Catti, M.; Dovesi, R.; Pavese, A.; Saunders, V. R . *J. Phys. Condens. Matter.* **1991**, *3*, 4151.

(33) (a) http://www.crystal.unito.it/Basis_Sets/Ptable.html. (b) Saadoune, I.; Cora, F.; Catlow, C. R. A. *J. Phys. Chem. B* **2003**, *107*, 3003.

(34) Amira, S.; Spångberg, D.; Hermansson, K. *J. Chem. Phys.* **2006**, *124*, 104501.

(35) Marcus, Y. *Chem. Rev.* **1988**, *88*, 1475.

(36) Lynch, B. J.; Y Zhao, Y.; Truhlar, D. G. *Phys. Chem. A* **2003**, *107*, 1384.

(37) Pavlov, M.; Siegbahn, P. E. M.; Sandström, M. *J. Phys. Chem. A* **1998**, *102*, 219.

(38) *CRC Handbook of Chemistry and Physics*, 73rd ed.; CRC Press; Boca Raton, FL, 1992.

(39) Soper, A. K.; Bruni, F.; Ricci, M. A. *J. Chem. Phys.* **1997**, *106*, 247.

(40) Rosseinsky, D. R. *Chem. Rev.* **1965**, *65*, 467.

(41) Lighstone, F. C.; Schwegler, E.; Hood, R. Q.; Gygi, F.; Galli, G. *Chem. Phys. Lett.* **2001**, *343*, 549.

(42) Sânchez-Marcos, E.; Pappalardo, R. R.; Rinaldi, D. *J. Phys. Chem.* **1991**, *95*, 8928.

JP801070B